Track-Following Control with Active Vibration Damping and Compensation of a Dual-Stage Servo System

Xinghui Huang, Roberto Horowitz and Yunfeng Li
Computer Mechanics Laboratory (CML)
Department of Mechanical Engineering
University of California at Berkeley, CA 94720

Abstract

This paper proposes a vibration control scheme for an actuated slider dual-stage servo system. The control scheme consists of three components: a basic track-following servo control loop, a feedback vibration damping loop of the voice coil motor (VCM) assembly and a plug-in feedforward vibration compensation loop for the microactuator (MA). A strain sensor located on the surface of the suspension, detects airflow-excited structural vibrations and its signal is fed to the feedback damping and feedforward compensation loops simultaneously. Because the strain sensor signal is analog, higher sampling control rates can be achieved for both the feedback damping and feedforward compensation controllers, than for the track-following servo loop, which is limited by the maximum attainable sampling rate of the position error signal (PES). Simulation results show that the track-misregistration (TMR) resulting from structural vibrations can be greatly attenuated using both the active feedback damping controller around the VCM and the feedforward vibration compensation controller on the MA, achieving and a total reduction of 43% in TMR over the conventional dual-stage actuation. This result implies that the proposed control scheme is suited for use in increasingly high track density, high performance hard disk drives.

1 Introduction

With the technological advances and breakthroughs in computer hard disk drives, there has been a continuing trend of increasing areal storage density from 100 Mb/in^2 in 1991 to 100 Gb/in^2, which was achieved recently, and toward the ultimate goal of 1 Tb/in^2 set by the information storage industry. It is predicted that future areal storage density increases will be achieved mainly through an increase in track density. For an areal density of 1 Tb/in^2, the corresponding track density is 500k-track per inch (TPI), which implies a track width of 50 nm and an allowable 3σ TMR of 5 nm.

To achieve this goal, the servo bandwidth has to be extended accordingly for better tracking performance. Dual-stage servo systems have been proposed for extended servo bandwidth. However, it is also expected that with the extended servo bandwidth and increased disk revolution speed, airflow-excited structural vibrations will become a significant obstacle to achieving higher track density. The structural vibration modes of the suspension are generally located at a frequency range that is higher than the available servo bandwidth, which is limited by the PES sampling rate. Thus, the TMR due to suspension vibrations can not be sufficiently attenuated with only the PES feedback control. On the contrary, with the extended servo bandwidth and further attenuation in the low frequency range, airflow excited structural vibrations may even be amplified according to Bode's integral theorem.

There exist several techniques for dealing with structural vibrations. The commonly used one is to insert notch filters in the control loop to ensure the stability of servo systems. However, notch filters generally reduce the phase margin and affect the system robustness [1]. Besides, notch filters just prevent the controller from exciting the assembly's vibration modes but cannot actively compensate for the airflow-excited structural vibrations.

The idea of utilizing additional sensors to further increase the actuator servo bandwidth has been explored by several researchers [2][3][4][5]. In [2][3], it was proposed to attach an acceleration sensor at a proper location in a hard disk drive to provide the feedforward vibration signal. The configurations in this paper are based on a single actuator, voice coil motor (VCM). Due to their single-stage configuration, the servo bandwidth cannot be significantly extended. In [5], active vibration damping of a PZT-actuated suspension dual-stage servo system was proposed and experimentally tested. The main disadvantage of this configuration compared to the actuated slider/head approach, is that the PZT actuators are located between the E-block arm and the suspension, and thus can excite structural vibration modes, which may limit its achievable bandwidth as compared to the actuated slider/head approach. Moreover, the resonance frequencies of PZT-actuated suspensions are generally lower than conventional suspensions and, as a consequence, are more susceptible to airflow-excited disturbances. For the actuated slider approach, active feedforward vibration compensation has been proposed [4]. Both of the above two approaches need additional vibration sensors to implement active vibration control. Since there is no limitation on the sampling rate of vibration signals, the vibration control loop is able to run at a higher rate than the PES feedback loop to achieve a higher bandwidth and hence better performance.

In this paper, a feedback plus feedforward control scheme is proposed for airflow-excited suspension vibration control. It is based on an actuated slider dual-stage servo system, which utilizes a MEMS MA located at the tip of the suspension. Vibration control is implemented by a feedback vibration damping loop of the VCM and a feedforward vibration compensation of the MA. Notch filters are not used in the track-following loop design because those vibration modes are already adequately suppressed by the VCM's vibration damping loop. This paper is organized as follows. Section 2

discusses the system structure and actuator and sensor modelling. The detailed design procedure and derivation of the proposed vibration control scheme are presented in Section 3. Simulation results and analysis are shown in Section 4. Conclusions are give in Section 5.

2 System Structure and Modelling

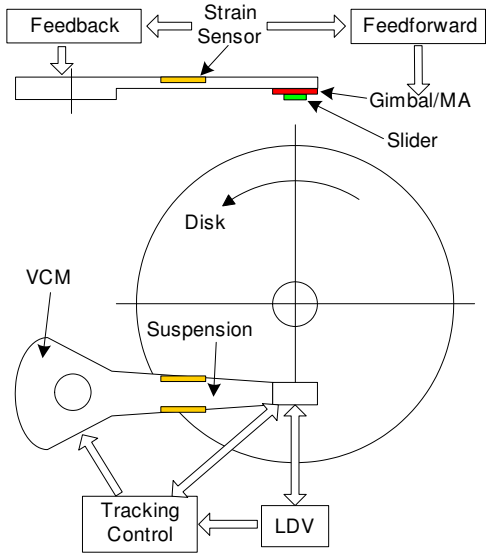

Figure 1: Dual-stage drive structure and suspension vibration measurement setup

Fig. 1 illustrates the proposed experimental control system configuration. It consists of two actuators: a VCM and an MA located between the suspension tip and the slider. The feedback loop in the lower part of the figure depicts the basic track-following servo loop, which only utilizes the PES measured by a laser doppler vibrometer (LDV)[1]. Strain sensors are attached or fabricated on the surface of the suspension for sensing structural vibrations. The vibration signal is both fed back to the VCM and fed forward to the MA for vibration control. The sensed vibrations not only are excited by the actuator inputs, but may also be excited by airflow disturbances. Therefore, airflow-excited structural vibrations are expected to be effectively attenuated with this control scheme.

2.1 VCM Assembly and Sensor Dynamics

The suspension model used in this simulation study was that of an actuated suspension that had been used in previous simulation and experimental studies [5]. We assume that one of the PZT elements in that suspension is used as a strain sensor. The second PZT actuator is not used. Instead, a MEMS MA is used to move the slider relative to the suspension. Figs. **??** shows the frequency responses from the VCM input to the head displacement and strain sensor output respectively. From this figure, we can see that the major vibration modes of the VCM-suspension assembly in our setup include the assembly butterfly mode (M1), the suspension sway

[1] In actual disk drives, the PES is measured by the magnetic head, not an LDV

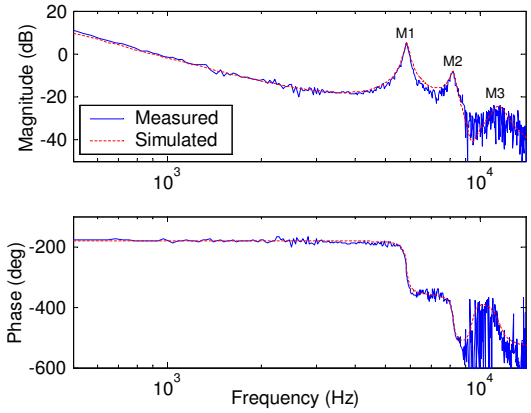

Figure 2: Frequency response from VCM input to head displacement

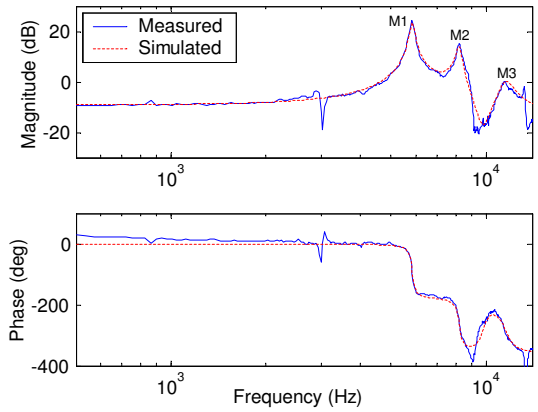

Figure 3: Frequency response from VCM input to PZT sensor output

mode (M2), and the suspension 1st torsion mode (M3). The butterfly mode results from the coupling of the in-plane sway modes of the E-block arm and the coil, in which they move out-of-phase with respect to each other about the pivot. From Fig. **??**, it can be seen that the strain sensor can pick up most of the off-track modes of the VCM-suspension assembly. As expected, the strain sensor does not sense the rigid body mode. These frequency responses can be modelled as a summation of the rigid body mode, several structural vibration modes and a direct feedthrough term. The general expression of such transfer functions can be written as

$$G_V(s) = \frac{A_0}{s^2} + \sum_{i=1}^{N} \frac{\omega_i^2 A_i}{s^2 + 2\zeta_i \omega_i s + \omega_i^2} + d\,, \qquad (1)$$

where A_0 is the gain of the rigid body mode, N is the total number of vibration modes being considered, ω_i, ζ_i and A_i are the natural frequency, the damping ratio, and the modal constant of mode i respectively, and d is the direct feedthrough term from input to output. These modal parameters can be identified from the measured frequency responses using modal testing techniques such as the peak-magnitude method. The dashed lines in the figures show the frequency responses of the identified model.

2.2 Microactuator Dynamics

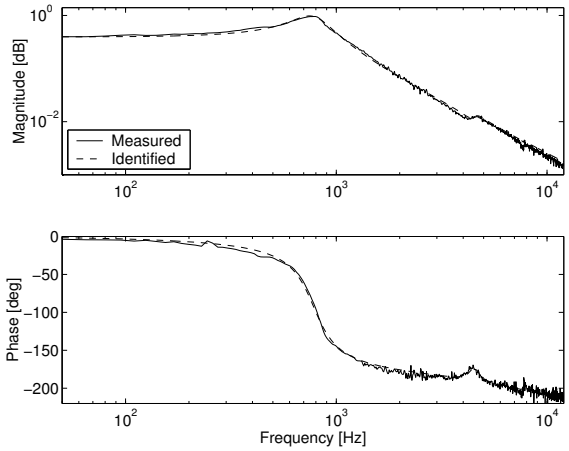

Figure 4: Open-loop frequency response of the microactuator

The MA model is obtained based on the experimental results of a prototype MEMS MA that was fabricated by our research group. It is an electrostatic translational MA. Its measured and identified frequency responses are shown in Fig. 4. From the figure, it is seen that the MA roughly has a single moderately damped vibration mode at around 1 kHz. Besides, there is a small peak at around 5 kHz. This peak results from the actuator's rotational mode. Redesign and fabrication are in progress to increase the vibration mode to about 3 kHz and effectively eliminate the rotational mode. Therefore, the MA can be modelled as a single mass-spring-damper system with satisfying precision:

$$G_M(s) = \frac{\omega^2 A}{s^2 + 2\zeta\omega s + \omega^2}\,. \tag{2}$$

2.3 Airflow-Excited Structural Vibrations

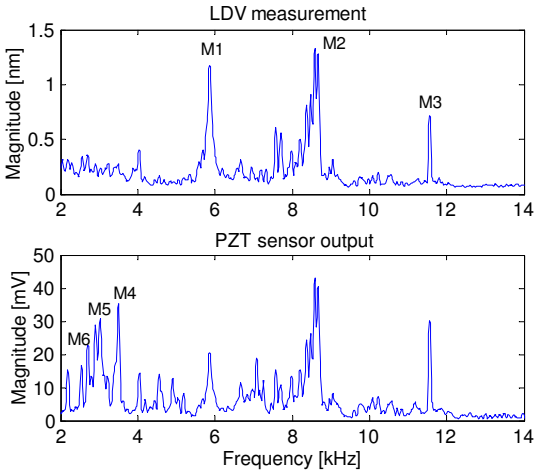

Figure 5: Frequency spectra of the head off-track motion and the PZT sensor output due to airflow-excited vibrations

Fig. 5 shows the frequency spectra of the head off-track motion and the strain sensor output when the disk is rotating at 7200-RPM and no control action is applied. As shown in the figure, the VCM assembly dynamics is dominated by the rigid body mode in the low frequency range and the structural vibration modes in the high frequency range. Three major off-track modes, denoted M1, M2 and M3, are excited by airflow disturbances. M1 is the VCM assembly butterfly mode, M2 is the suspension sway mode and M3 is the suspension 1st torsion mode. The strain sensor is able to sense these three modes. Besides, the sensor also picks up some non-off-track modes: M4, M5 and M6, and they do not show up in the head off-track motion. These modes are probably due to the bending modes of the suspension and are excited by the airflow disturbance in the out-of-plane direction. To implement off-track motion control, those non-off-track modes need to be filtered out in controller design.

2.4 The Complete Model

Combining the dynamics of the VCM assembly and strain sensor, and including the airflow-excited structural vibration modes, a 2-input-2-output system can be obtained in state space form:

$$\begin{bmatrix}\dot{\boldsymbol{x}}\\ \dot{\boldsymbol{x}}_w\\ \dot{\boldsymbol{x}}_m\end{bmatrix} = \begin{bmatrix}A & 0 & 0\\ 0 & A_w & 0\\ 0 & 0 & A_m\end{bmatrix}\begin{bmatrix}\boldsymbol{x}\\ \boldsymbol{x}_w\\ \boldsymbol{x}_m\end{bmatrix} + \begin{bmatrix}B & 0\\ 0 & 0\\ 0 & B_m\end{bmatrix}\begin{bmatrix}u_v\\ u_m\end{bmatrix} + \begin{bmatrix}B_{w1}\\ B_{w2}\\ 0\end{bmatrix}\boldsymbol{w}\,,$$
$$\begin{bmatrix}y_h\\ y_p\end{bmatrix} = \begin{bmatrix}C_1 & 0 & C_m\\ C_2 & C_w & 0\end{bmatrix}\begin{bmatrix}\boldsymbol{x}\\ \boldsymbol{x}_w\\ \boldsymbol{x}_m\end{bmatrix} + \begin{bmatrix}D_1 & 0\\ D_2 & 0\end{bmatrix}\begin{bmatrix}u_v\\ u_m\end{bmatrix}\,, \tag{3}$$

where $\boldsymbol{x}$ and $\boldsymbol{x}_w$ are the states of off-track and non-off-track modes of the VCM-suspension assembly, respectively, $\boldsymbol{x}_m$ is the state of the MA, u_v and u_m are the control inputs to the VCM and MA respectively, $\boldsymbol{w}$ denotes airflow disturbances, y_h and y_p are the head displacement and sensor output respectively.

3 Controller Design

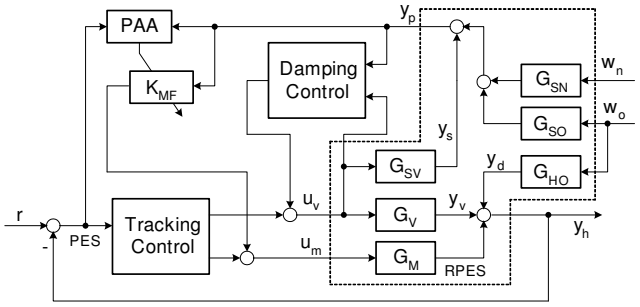

Figure 6: Block diagram of the control system

The proposed overall control structure is based on the block diagram shown in Fig. 6. The part inside the dashed box is the augmented plant model with airflow disturbances. The controller consists of three main loops: a feedback vibration damping loop, a feedforward vibration compensation loop and a track-following servo control loop. w_o and w_n represent off-track and non-off-track airflow disturbances respectively. The PZT sensor picks up information from both airflow disturbances and the VCM input u_v.

Since dedicated sensor is used for vibration detection, its sampling rate will not be limited by that of PES. A higher sampling rate of the vibration signal is advantageous for achieving high actuation bandwidth in high-frequency vibration control. The MA generates the relative motion, $RPES$, to compensate for the remaining tracking errors of the VCM. Besides the structural vibrations, r denotes all the track runout coming from various sources.

3.1 Vibration Damping Control Design

The vibration damping control block is designed using the LQG method. First, a discrete-time model is obtained based on the augmented plant model. The computational time delay is also incorporated in the discrete-time model for better state estimation. Then a Kalman filter is derived based on this model. The discrete-time model of the plant in Eq. 3, with computational time delay T_d, can be obtained as follows:

$$\begin{aligned}\begin{bmatrix}\boldsymbol{x}(k+1)\\ \boldsymbol{x}_w(k+1)\end{bmatrix} &= \begin{bmatrix}\Phi & 0\\ 0 & \Phi_w\end{bmatrix}\begin{bmatrix}\boldsymbol{x}(k)\\ \boldsymbol{x}_w(k)\end{bmatrix}\\ &\quad + \begin{bmatrix}\Gamma_{sd} & \Gamma_d\\ 0 & 0\end{bmatrix}\begin{bmatrix}u_v(k)\\ u_v(k-1)\end{bmatrix} + \begin{bmatrix}\Gamma_{w1}\\ \Gamma_{w2}\end{bmatrix}\boldsymbol{w}(k)\,,\\ y_p(k) &= \begin{bmatrix}C_2 & C_w\end{bmatrix}\begin{bmatrix}\boldsymbol{x}(k)\\ \boldsymbol{x}_w(k)\end{bmatrix} + \begin{bmatrix}0 & D_2\end{bmatrix}\begin{bmatrix}u_v(k)\\ u_v(k-1)\end{bmatrix} + v(k)\,,\end{aligned} \tag{4}$$

where $v(k)$ is the sensor measurement noise, and

$$\begin{aligned}\Phi &= e^{AT_s}, \qquad \Gamma_{sd} = \textstyle\int_{T_d}^{T_s} e^{A\tau}B d\tau,\\ \Phi_w &= e^{A_w T_s}, \quad \Gamma_d = \textstyle\int_0^{T_d} e^{A\tau}B d\tau.\end{aligned}$$

Γ_d just reflects the effect of the computation delay. In this Kalman filter model, two design parameters can be tuned to set the bandwidth of the observer: the covariance matrix W of airflow disturbances and the measurement noise covariance matrix V.

Based on the separation principle of LQG control, the design of the feedback control is also based on this model with some state rearrangements. Since at time instant k, $u_v(k-1)$ is already known, therefore it can be put in the state vector leaving the only control input $u_v(k)$ to be determined:

$$\begin{aligned}\begin{bmatrix}\boldsymbol{x}(k+1)\\ \boldsymbol{x}_w(k+1)\\ u_v(k)\end{bmatrix} &= \begin{bmatrix}\Phi & 0 & \Gamma_d\\ 0 & \Phi_w & 0\\ 0 & 0 & 0\end{bmatrix}\begin{bmatrix}\boldsymbol{x}(k)\\ \boldsymbol{x}_w(k)\\ u_v(k-1)\end{bmatrix} + \begin{bmatrix}\Gamma_{sd}\\ 0\\ I\end{bmatrix}u_v(k)\,,\\ y_h(k) &= \begin{bmatrix}C_1 & 0 & D_1\end{bmatrix}\begin{bmatrix}\boldsymbol{x}(k)\\ \boldsymbol{x}_w(k)\\ u_v(k-1)\end{bmatrix}.\end{aligned} \tag{5}$$

The cost function for this LQ design is

$$J = \sum_k \left\{y_h^2(k) + Ru_v^2(k)\right\}\,, \tag{6}$$

in which the control action weight R can be tuned to achieve the desired system responses. Fig. 7 shows the simulation results of the damped transfer function of the VCM assembly. Note that M1 and M2 have been effectively damped with the damping action. While there is no effect on M3 due to its small magnitude.

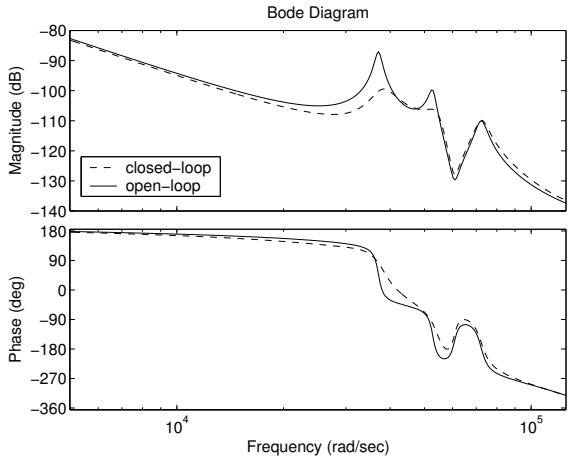

Figure 7: Bode plot of the VCM assembly with/without damping control

3.2 Feedforward Compensation Design

In addition to feedback damping of structural vibrations, the remaining vibrations can further be compensated by the MA. Since the MA is located between the suspension tip and the slider, its action will have little effect on structural vibrations. Therefore, feedforward compensation is needed to compensate for it so that the net vibration at the slider or read-write head is minimized. Due to the time-varying property of airflow disturbances, adaptive control is designed for feedforward vibration compensation of the MA.

The feedforward compensator, K_{MF}, assumes a finite impulse response (FIR) for stability consideration:

$$K_{MF}(\theta, q^{-1}) = h_0 + h_1 q^{-1} + \cdots + h_n q^{-n}\,, \tag{7}$$

where θ is the filter coefficient vector $\theta = [h_0\, h_1 \cdots h_n]^T$. The output of the MA from the feedforward control can be expressed as

$$\begin{aligned}y_{MF}(k) &= G_M(q^{-1})K_{MF}(q^{-1})y_p(k)\\ &= K_{MF}(q^{-1})G_M(q^{-1})y_p(k)\\ &= K_{MF}(q^{-1})x_f(k)\\ &= \theta^T\phi(k-1)\,,\end{aligned} \tag{8}$$

where $x_f(k) = G_M(q^{-1})y_p(k)$ and $\phi(k) = [x_f(k)\, x_f(k-1)\cdots x_f(k-n)]^T$. Since $x_f(k)$ is not directly measurable, it is estimated by passing $y_p(k)$ through the model of the MA, $\hat{G}_M$:

$$x_f(k) = \hat{G}_M(q^{-1})y_p(k)\,. \tag{9}$$

The recursive least squares (RLS) method can be applied for parameter adaptation and θ is tuned such that the overall tracking error, PES, is minimized.

3.3 Tracking-Following Control Design

There are several popular techniques for designing dual-stage track-following controllers. In this paper, a relatively straightforward method, called the sensitivity function decoupling method or the series compensator, is used [6][7].

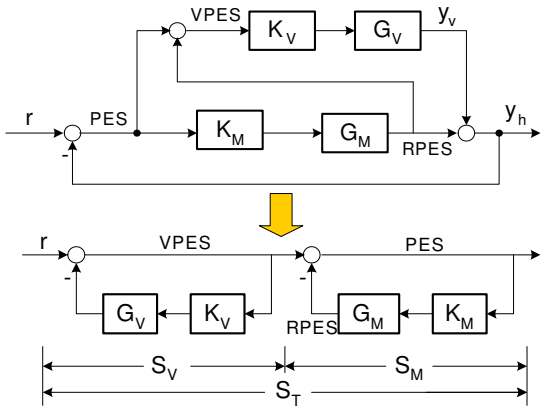

Figure 8: Block diagram of the track-following controller

Fig. 8 shows the block diagram of a dual-stage track-following controller using this design method. Decoupling of the whole sensitivity function is achieved by adding PES and $RPES$ together before sending it to the VCM controller K_V. Straightforward manipulation shows that the total closed-loop sensitivity function can be expressed as a cascade of the sensitivity functions of VCM and MA, i.e.,

$$S_T = S_V \cdot S_M \,. \tag{10}$$

With S_T decoupled, K_V and K_M can be designed sequentially using conventional design techniques, such as pole placement. After decoupling, it is clear that $VPES$ is the tracking error with the VCM actuator solely; while the MA does further compensation to yield the final error, PES. "Dual stage" can best be illustrated in this design. It is also noted that $RPES$, the motion of the MA relative to that of the VCM, should be available for decoupling. Capacitive sensing structure can be embedded in the MA to measure $RPES$. Otherwise, this value needs to be estimated based on the MA model.

4 Simulation Results

Simulation results are obtained using the proposed vibration control scheme. In the simulation, the designed crossover frequencies are 700 Hz for the VCM and 3500 Hz for the MA, respectively. Dual-rate sampling is assumed, in which PES is available at 25 kHz, while $RPES$ is available at 50 kHz.

4.1 Comparison between Various Configurations

First, the tracking performance for various system configurations is compared. Track runout r is generated with a combination of various disturbance sources. Measurement noises, control input disturbances are injected into the system at proper locations. The performance is indicated by the 1-σ value of PES. The simulation results are shown in Fig. 9. In the figure, DS means the basic dual-stage track-following control without any vibration control; LQG means the vibration feedback damping control of the VCM assembly; FF means the feedforward vibration compensation of the MA. Different combination implies different configuration of control schemes. From the figure, we can see that with only the DS control, there are two major vibration peaks resulting from VCM assembly butterfly mode M1 and suspension 1st torsion mode M2. With extended servo bandwidth and more attenuation in the low frequency range, these vibration modes get amplified. Both feedback damping control and feedforward compensation can attenuate these modes. But in LQG, some regions between the peaks get amplified; while in FF, some non-off-track modes show up. The combination of LQG and FF yields the best performance, from 14 nm for DS to 9.17 nm for DS_LQG_FF.

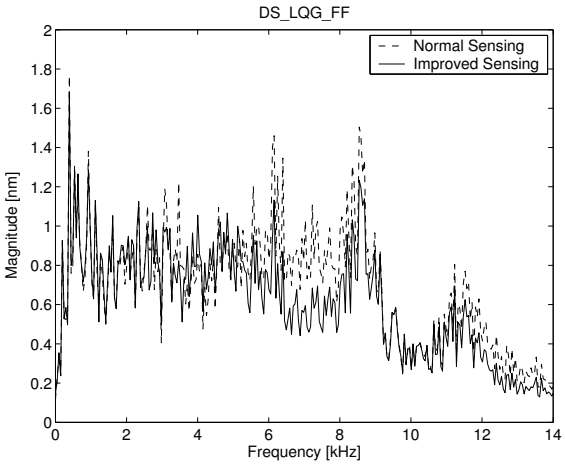

Figure 10: Performance comparison between normal/improved sensing

4.2 Normal Sensing vs Improved Sensing

Further improvement can be achieved if the sensing quality can be improved. Normally, the PZT sensor picks up both off-track and non-off-track vibration modes. Improved sensing means that the sensor only picks up those off-track modes while be insensitive to those non-off-track modes. This may be achieved by optimizing the sensor in its location, orientation and shape [8]. The performance comparison is shown in Fig. 10. It is seen that with improved sensing, the vibration peaks can be further attenuated and the $\sigma(PES)$ is decreased from 9.17 nm for normal sensing to 8.03 nm for improved sensing, while the total improvement from DS to DS_LQG_FF is 43%. Fig. 11 shows the performance for all those configurations.

5 Conclusions

In this paper, a track-following controller design with active vibration damping and compensation has been proposed for a VCM-MEMS MA dual-stage servo system. Vibration control is realized by a plug-in feedback damping loop of the VCM assembly and a plug-in feedforward compensation loop of the MA. The feedback damping loop is designed using the LQG technique, while the feedforward compensation part is based on an adaptive control structure. Simulation results show the effectiveness of the proposed control scheme in attenuating airflow-excited structural vibrations and enhancing the overall performance of the servo system.

Simulation study also shows the potential improvement with improved sensing, in which the vibration sensor only senses those PES-related off-track vibration modes, while be insensitive to those

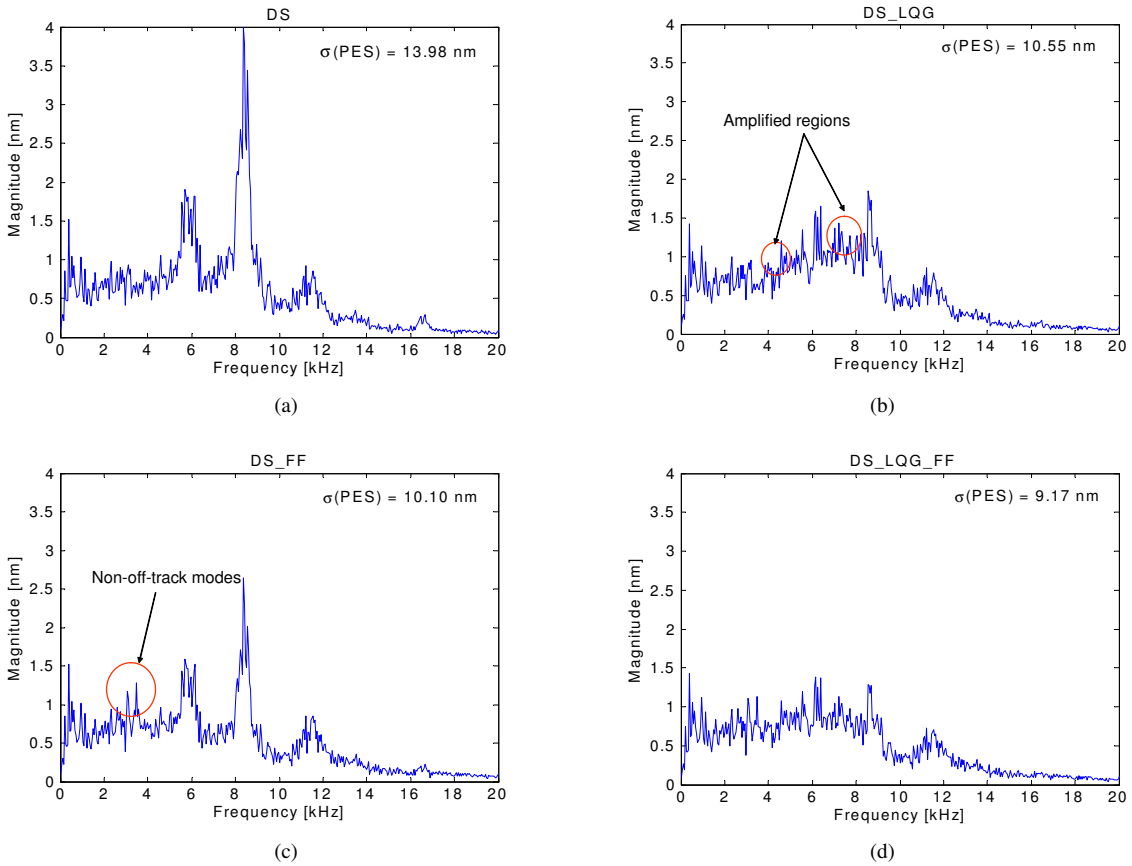

Figure 9: Simulation results for various system control schemes: (a) Only with track-following control; (b) Track-following plus feedback vibration damping; (c) Track-following plus feedforward vibration compensation; (d) Track-following with vibration damping and compensation.

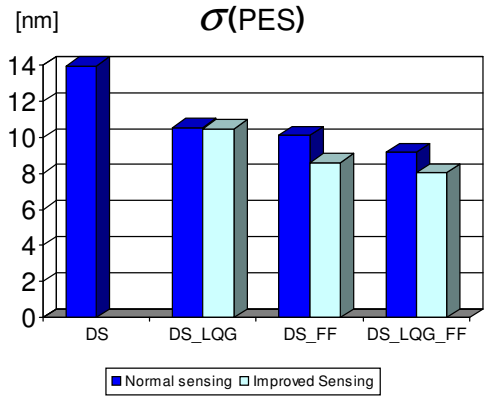

Figure 11: Performance comparison between various configurations

non-off-track modes. Besides, with improved sensing, the LQG control design will also be simplified since those non-off-track modes do not have to be modelled any more and therefore less computation time is needed. Optimization in sensor location, orientation and shape has become an important topic in sensor design and fabrication.

We are currently doing preliminary testing and integration of the MA. Redesign, optimization, and fabrication of the MA and vibration sensors are also in progress. Experiments will be conducted to verify all those designs and predictions of the proposed vibration control scheme.

References

[1] F. Y. Huang, T. Semba, W. Imaino, and F. Lee, "Active damping in hdd actuator," *IEEE Transactions on Magnegics*, vol. 37, no. 2, pp. 847–849, March 2001.

[2] S. Pannu and R. Horowitz, "Increased disturbance rejection for hard disk drives using accelerometers," *The Journal of Information Storage and Processing Systems*, vol. 1, pp. 95–103, 1999.

[3] R. Oboe, "Use of low-cost mems accelerometers for vibration compensation in hard disk drives," in *Proceedings of the 6th International Workshop on Advanced Motion Control*, 2000.

[4] Y. Li and R. Horowitz, "Active suspension vibration control with dual-stage actuators in hard disk drives," in *Proceedings of American Control Conference*, vol. 4, 2001, pp. 2786–2791.

[5] Y. Li, F. Marcassa, R. Horowitz, R. Oboe, and R. Evans, "Track-following control with active vibration damping of a pzt-actuated suspension dual-stage servo system," in *Proceedings of American Control Conference*, vol. 3, 2003.

[6] K. Mori, T. Munemoto, H. Otsuki, Y. Yamaguchi, and K. Akagi, "A dual-stage magnetic disk drive actuator using a piezoelectric device for a high track density," *IEEE Transactions on Magnetics*, vol. 27, pp. 5298–5300, Nov. 1991.

[7] Y. Li and R. Horowitz, "Mechatronics of electrostatic microactuators for computer disk drive dual-stage servo systems," *IEEE/ASME Transactions on Mechatronics*, vol. 6, no. 2, pp. 111–121, 2001.

[8] Y. Huang, M. Banther, P. D. Mathur, and W. Messner, "Design and analysis of a high bandwidth disk drive servo system using an instrumeted suspension," *IEEE/ASME Transaction of Mechatronics*, vol. 4, no. 2, pp. 196–206, 1999.